

# Catalysis Science & Technology

Accepted Manuscript



This is an *Accepted Manuscript*, which has been through the Royal Society of Chemistry peer review process and has been accepted for publication.

*Accepted Manuscripts* are published online shortly after acceptance, before technical editing, formatting and proof reading. Using this free service, authors can make their results available to the community, in citable form, before we publish the edited article. We will replace this *Accepted Manuscript* with the edited and formatted *Advance Article* as soon as it is available.

You can find more information about *Accepted Manuscripts* in the [Information for Authors](#).

Please note that technical editing may introduce minor changes to the text and/or graphics, which may alter content. The journal's standard [Terms & Conditions](#) and the [Ethical guidelines](#) still apply. In no event shall the Royal Society of Chemistry be held responsible for any errors or omissions in this *Accepted Manuscript* or any consequences arising from the use of any information it contains.

# Selective Gas Phase Hydrogenation of Nitroarenes over Mo<sub>2</sub>C Supported Au-Pd

Xiaodong Wang<sup>a1</sup>, Noémie Perret<sup>a</sup>, Laurent Delannoy<sup>b,c</sup>,  
Catherine Louis<sup>b,c</sup> and Mark A. Keane<sup>a,\*</sup>

<sup>a</sup>Chemical Engineering, School of Engineering & Physical Sciences,  
Heriot-Watt University, Edinburgh EH14 4AS, Scotland

<sup>b</sup>Sorbonne Universités, UPMC Univ Paris 06, UMR 7197, Laboratoire de Réactivité  
de Surface, 4 Place Jussieu, F-75005, Paris, France

<sup>c</sup>CNRS, UMR 7197, Laboratoire de Réactivité de Surface, 4 Place Jussieu, F-75005,  
Paris, France

\*corresponding author

Tel: +44(0)131 451 4719, e-mail: [M.A.Keane@hw.ac.uk](mailto:M.A.Keane@hw.ac.uk)

<sup>1</sup>present address: School of Engineering, University of Aberdeen, Aberdeen AB24 3UE,  
Scotland

## Abstract

We report the first synthesis of Mo<sub>2</sub>C-supported Au and Au-Pd catalysts (nominal Au/Pd = 10 and 30) obtained from colloidal nanoparticles stabilised by polyvinyl alcohol (PVA). Equivalent Au/Al<sub>2</sub>O<sub>3</sub> and Au-Pd/Al<sub>2</sub>O<sub>3</sub> were prepared and served as benchmark. Residual PVA was removed by thermal treatment in N<sub>2</sub>, which was monitored by thermogravimetric analysis. The catalysts were characterised in terms of temperature programmed reduction (TPR), BET surface area, H<sub>2</sub> chemisorption, powder X-ray diffraction (XRD), X-ray photoelectron spectroscopy (XPS) and transmission electron microscopy (TEM) measurements. The reduced catalysts exhibited an equivalent metal particle size range (1-8 nm) and mean (4-5 nm). The carbide samples showed greater H<sub>2</sub> chemisorption capacity than the Al<sub>2</sub>O<sub>3</sub> systems where inclusion of Pd enhanced H<sub>2</sub> uptake. XPS measurements suggest electron transfer from Al<sub>2</sub>O<sub>3</sub> to Au while the Au binding energy for the carbide samples is close to the metallic Au reference. The catalysts were tested in the gas phase hydrogenation of nitrobenzene, *p*-chloronitrobenzene and *p*-nitrobenzonitrile and delivered 100% selectivity to the target amine in each case. Inclusion of Pd served to increase selective hydrogenation rate where Au-Pd/Mo<sub>2</sub>C outperformed Au-Pd/Al<sub>2</sub>O<sub>3</sub>, a response that is attributed to increased surface hydrogen.

**Keywords:** Mo<sub>2</sub>C; Al<sub>2</sub>O<sub>3</sub>; Au-Pd bimetallic catalysts; gas phase hydrogenation; nitrobenzene; *p*-chloronitrobenzene; *p*-nitrobenzonitrile.

## 1. Introduction

The use of bimetallic catalysts is experiencing increased research interest<sup>1</sup> due to enhanced activity<sup>2,3</sup>, selectivity<sup>4</sup> and resistance to poisoning<sup>5</sup> when compared with corresponding mono-metallic systems. This has been exploited in commercial applications, notably Pd-Zn in hydrogen production,<sup>6</sup> Pd-Au in vinyl acetate synthesis,<sup>7</sup> Cu-Zn in methanol production<sup>8</sup> and Fe-Cr in the water gas shift reaction<sup>9</sup>. This study focuses on Au-Pd formulations, which to date have been used in the synthesis of hydrogen peroxide,<sup>10</sup> NO<sub>2</sub> decomposition,<sup>11</sup> hydrodesulphurisation (of thiophene and dibenzothiophene),<sup>12</sup> hydrodechlorination (of trichloroethene),<sup>13</sup> oxidation (of glycerol,<sup>14</sup> CO,<sup>15</sup> benzyl alcohol, cinnamyl alcohol, 2-octen-1-ol and *n*-octanol)<sup>16</sup> and hydrogenation (of 1,3-butadiene,<sup>17,18</sup> benzaldehyde,<sup>5</sup> naphthalene and toluene,<sup>19,20</sup> acetylene,<sup>21</sup> allyl alcohol<sup>2</sup> and cinnamaldehyde<sup>22</sup>). Improved performance relative to monometallic Pd and Au catalysts has been attributed to ensemble, ligand or geometric effects.<sup>23,24</sup> Prior studies have established chemoselectivity for supported Au in targeted –NO<sub>2</sub> reduction in functionalised nitro-compounds.<sup>25-28</sup> Reaction exclusivity is important in minimising waste and addressing the sustainability gap in non-selective processes using standard (Pd,<sup>29</sup> Ru<sup>30</sup> or Ni<sup>31</sup>) transition metal catalysts. However, hydrogenation rates delivered by supported Au fall below those achieved with non-selective metal catalysts.<sup>32</sup> It is now crucial to increase selective hydrogenation rate to address the key commercial consideration of productivity that combines activity and selectivity. Gold activation of H<sub>2</sub> is the limiting step due to the high energy barrier for dissociative adsorption.<sup>33</sup> We have explored the use of Mo<sub>2</sub>C as a support that can chemisorb H<sub>2</sub> and increase surface concentration, leading to higher hydrogenation rates.<sup>34</sup> We demonstrated higher selective hydrogenation rates over Au/Mo<sub>2</sub>C than Au/Al<sub>2</sub>O<sub>3</sub> but further improvements are required in Au/Mo<sub>2</sub>C synthesis directed at decreasing Au particle size as a critical variable that governs H<sub>2</sub> activation.<sup>33</sup> Preliminary data<sup>3</sup> established that addition of Pd to Au on Al<sub>2</sub>O<sub>3</sub> (prepared by

deposition-precipitation) increased hydrogenation activity but lower selectivities were recorded at higher Pd loading ( $\text{Au/Pd} < 20$ ). We have now examined the viability of  $\text{Mo}_2\text{C}$ -supported Au-Pd to elevate rate while retaining selectivity in the hydrogenation of nitroarenes.

The challenge in supported bimetallic synthesis is to exert control over surface composition and size/dispersion.<sup>35</sup> To date, supported Au-Pd catalysts have principally been prepared by impregnation (incipient<sup>19</sup> and wet<sup>3,5,17</sup>) and (co)-deposition<sup>3,10,17,36,37</sup>. The synthesis procedure influences ultimate metal loading, morphology and structure<sup>10,21</sup> where surface segregation and formation of isolated Au and Pd particles can occur<sup>3</sup>. Use of Au-Pd catalysts has largely focused on Au addition to modify Pd catalytic properties, where  $\text{Au/Pd} < 1$ .<sup>21</sup> This study takes the opposite approach with Pd inclusion directed at increasing selective hydrogenation rate. A range of oxides ( $\text{Fe}_2\text{O}_3$ ,<sup>37</sup>  $\text{TiO}_2$ ,<sup>38</sup>  $\text{ZrO}_2$ <sup>10</sup> and  $\text{MgO}$ <sup>13</sup>) have been used as Au-Pd support with the predominance of  $\text{Al}_2\text{O}_3$ <sup>3,13,17,19,20,37</sup> and  $\text{SiO}_2$ <sup>13,20,21,36,39</sup> as carriers. In this study, we report the first preparation of Au-Pd/ $\text{Mo}_2\text{C}$  ( $\text{Au/Pd} \geq 10$ ) using colloidal polyvinyl alcohol (PVA), which provides a protective layer around the metal nanoparticles preventing agglomeration in solution to generate small supported metal particles.<sup>40</sup> Use of “protecting” agents (polyvinyl pyrrolidone (PVP)<sup>12</sup> and PVA<sup>14,16</sup>) to minimise nanoparticle aggregation has been applied in the synthesis of supported Au,<sup>41</sup> Pd<sup>42</sup> and Au-Pd<sup>14,16</sup>. We examine the catalytic action of Au-Pd/ $\text{Mo}_2\text{C}$  in the hydrogenation of nitroarenes (nitrobenzene, *p*-chloronitrobenzene and *p*-nitrobenzonitrile) where Au-Pd/ $\text{Al}_2\text{O}_3$  prepared using the same method served as benchmark.

## 2. Experimental

### 2.1 Chemicals

Gold (III) chloride hydrate ( $\text{HAuCl}_4 \cdot x\text{H}_2\text{O}$ , 99.999%), palladium tetraamine dinitrate ( $\text{Pd}(\text{NH}_3)_4(\text{NO}_3)_2$ , 99.99%) and polyvinyl alcohol (PVA, 87-89%) were obtained from Aldrich,

molybdic acid ( $\text{H}_2\text{MoO}_4$ , 99%) and  $\text{NaBH}_4$  (>99%) from Merck and Fluka, respectively. All gases were of high purity (99.9%) and supplied by BOC or Air Liquide. The nitro-reactants (nitrobenzene, *p*-chloronitrobenzene and *p*-nitrobenzonitrile, Aldrich ( $\geq 98\%$ )) and solvent (1-butanol, Riedel-de Haen, 99.8%) were used as received without further purification.

## 2.2 Catalyst Preparation

$\beta\text{-Mo}_2\text{C}$  was synthesised *via* temperature programmed carburisation of  $\text{H}_2\text{MoO}_4$  (2 g) in 20 % v/v  $\text{CH}_4$  in  $\text{H}_2$  ( $340 \text{ cm}^3 \text{ min}^{-1}$ ). The temperature was ramped at  $1 \text{ K min}^{-1}$  to 973 K, maintained for 1 h and cooled to ambient temperature under  $\text{H}_2$  with sample passivation in 1 % v/v  $\text{O}_2/\text{He}$  ( $30 \text{ cm}^3 \text{ min}^{-1}$ ) for 1 h. The passivation step was necessary to circumvent autothermal oxidation upon contact with air.<sup>43</sup> Gold and gold-palladium catalysts were prepared according to a colloidal method developed by Prati *et al.*<sup>44</sup> for carbon supports and adopted for use with  $\text{Al}_2\text{O}_3$ . Gold was incorporated using an Au sol that was deposited on  $\text{Mo}_2\text{C}$  (or  $\text{Al}_2\text{O}_3$ ) with a nominal loading of 1 % w/w as reported previously.<sup>18</sup> Aqueous solutions of  $\text{HAuCl}_4$  ( $6 \text{ cm}^3$ ,  $2.5 \times 10^{-2} \text{ M}$ ) and PVA ( $1.5 \text{ cm}^3$ ,  $2.3 \times 10^{-6} \text{ M}$ ;  $\text{Au/PVA} = 50$ ) were added to  $200 \text{ cm}^3$  distilled water with vigorous agitation for 3 min, a freshly prepared solution of  $\text{NaBH}_4$  ( $4.5 \text{ cm}^3$ ,  $0.1 \text{ M}$ ) was added ( $\text{NaBH}_4/\text{Au} = 3$ ) with a resultant colour change from light yellow to red, indicating reduction of  $\text{Au}^{3+}$  to  $\text{Au}^0$ . The sol was acidified to  $\text{pH} = 2$  with  $\text{H}_2\text{SO}_4$  ( $0.1 \text{ M}$ ) and 3 g support added to the mixture, which was maintained under vigorous stirring at ambient temperature for 2 h; water was removed on a rotary evaporator. Bimetallic synthesis followed an equivalent protocol where 1 % w/w  $\text{Au/Mo}_2\text{C}$  (or  $\text{Au/Al}_2\text{O}_3$ ) was suspended in  $200 \text{ cm}^3$  distilled water to which a known amount of PVA solution ( $2.3 \times 10^{-6} \text{ M}$ ;  $\text{Pd/PVA} = 80$ ) was added under vigorous stirring with subsequent addition of  $\text{Pd}(\text{NH}_3)_4(\text{NO}_3)_2$  ( $4.7 \times 10^{-3} \text{ M}$ ; nominal  $\text{Au/Pd} = 10$  or 30). Hydrogen ( $50 \text{ cm}^3 \text{ min}^{-1}$ ) was then bubbled into the reactor for 2 h to reduce Pd on the supported Au colloids. The mixture was

stirred for a further 16 h and water removed by rotary evaporation. The resultant solid was washed repeatedly and dried under vacuum at ambient temperature. The samples were heated ( $2 \text{ K min}^{-1}$ ) in  $600 \text{ cm}^3 \text{ min}^{-1} \text{ N}_2$  to 773 K for 1 h to remove the stabilising agents, cooled to ambient temperature and subjected to thermal reduction in  $100 \text{ cm}^3 \text{ min}^{-1} \text{ H}_2$  to 773 K (at  $2 \text{ K min}^{-1}$ ). Upon cooling, the samples were passivated as above for off-line analysis. The bimetallic catalysts are labelled as Au-Pd/Mo<sub>2</sub>C (or Al<sub>2</sub>O<sub>3</sub>)-X, where X represents the nominal Au/Pd molar ratio (= 10 or 30).

### 2.3 Catalyst Characterisation

The Au, Mo, Cl and Al contents were measured by inductively coupled plasma (ICP) atom emission spectroscopy (CNRS Centre of Chemical Analysis, Vernaison). Carbon content was determined using an Exeter CE-440 Elemental Analyser after sample combustion at 1873 K. Temperature programmed reduction (TPR), BET surface area and H<sub>2</sub> chemisorption were measured using the commercial CHEM-BET 3000 (Quantachrome) unit. The passivated samples were loaded into a U-shaped Quartz cell ( $10 \text{ cm} \times 3.76 \text{ mm i.d.}$ ) and heated in  $17 \text{ cm}^3 \text{ min}^{-1}$  (Brooks mass flow controlled) 5% v/v H<sub>2</sub>/N<sub>2</sub> at  $2 \text{ K min}^{-1}$  to  $523 \pm 1 \text{ K}$ , which was held for 1 h. The effluent gas passed through a liquid N<sub>2</sub> trap and H<sub>2</sub> consumption was monitored by TCD with data acquisition/manipulation using the TPR Win<sup>TM</sup> software. The samples were swept with  $65 \text{ cm}^3 \text{ min}^{-1} \text{ N}_2$  for 1.5 h, cooled to ambient temperature and subjected to H<sub>2</sub> chemisorption using a pulse (10  $\mu\text{l}$ ) titration procedure. BET surface area was determined (post TPR) in 30% v/v N<sub>2</sub>/He using pure N<sub>2</sub> (99.9%) as internal standard. At least three cycles of N<sub>2</sub> adsorption-desorption in the flow mode were employed to determine total surface area using the standard single point method. BET area and H<sub>2</sub> chemisorption measurements were reproducible to within  $\pm 3\%$  and the values quoted represent the mean.

Powder X-ray diffractograms (XRD) were recorded on a Bruker/Siemens D500 incident X-ray diffractometer using Cu K $\alpha$  radiation. The samples were scanned at 0.02° step<sup>-1</sup> over the range 20° ≤ 2 $\theta$  ≤ 85° and the diffractograms identified using JCPDS-ICDD reference standards, *i.e.* Au (Card No. 04-0784), Pd (05-0681),  $\beta$ -Mo<sub>2</sub>C (11-0680) and  $\delta$ -Al<sub>2</sub>O<sub>3</sub> (16-394). Thermogravimetric analysis (TGA) and differential scanning calorimetry (DSC) measurements were conducted using a SDT Q600 simultaneous TGA/DSC analyser (TA Instruments) that measured temporal mass and heat flow as a function of temperature. Samples were swept with air/N<sub>2</sub> (100 cm<sup>3</sup> min<sup>-1</sup>) and ramped (10 K min<sup>-1</sup>) from ambient temperature to 373 K with an isothermal hold (for 1 h) and subsequent heating to 773 K. Transmission electron microscopy (TEM) was performed using a JEOL 2010 electron microscope operating at 200 kV. Samples for analysis were crushed, homogenously dispersed in ethanol by ultrasonication and a drop of the suspension deposited on a carbon-coated copper grid and evaporated. Up to 200 individual Au particles were counted for each catalyst and the mean metal particle sizes are given as the surface area-weighted average ( $d$ ) according to

$$d = \frac{\sum_i n_i d_i^3}{\sum_i n_i d_i^2} \quad (1)$$

where  $n_i$  is the number of particles of diameter  $d_i$ . XPS spectra were collected on a SPECS (Phoibos MCD 150) x-ray photoelectron spectrometer using an Al K $\alpha$  ( $h\nu = 1486.6$  eV) x-ray source. The binding energies (BE) were calibrated with respect to the C-C/C-H component of the C 1s peak (BE = 284.7 eV). Spectra processing applied the Casa XPS software package.

#### 2.4 Catalytic Procedure

Reactions were carried out at 493 K and 1 atm, immediately after catalyst activation in H<sub>2</sub> (60 cm<sup>3</sup> min<sup>-1</sup>, 2 K min<sup>-1</sup> to 523 K, hold for 1 h) in a continuous flow fixed bed vertical glass



reactor (i.d. = 15 mm,  $l$  = 600 mm). The catalytic reactor and operating conditions to ensure negligible heat/mass transport limitations have been fully described elsewhere.<sup>45</sup> A layer of borosilicate glass beads served as a preheating zone, ensuring that the organic reactants were vaporised and reached reaction temperature before contacting the catalyst. Isothermal conditions ( $\pm 1$  K) were ensured by diluting the catalyst bed with ground glass (75  $\mu\text{m}$ ). Reaction temperature was continuously monitored by a thermocouple inserted in a thermowell within the catalyst bed. The reactant (nitrobenzene, *p*-chloronitrobenzene or *p*-nitrobenzonitrile) in butanol (as carrier) was delivered *via* a glass/teflon air-tight syringe and teflon line using a microprocessor controlled infusion pump (Model 100 kd Scientific) at a fixed flow rate. A co-current flow of organic and  $\text{H}_2$  ( $400 \leq \text{H}_2/\text{nitroarene} \leq 2500$ ) was maintained at  $GHSV = 2 \times 10^4 \text{ h}^{-1}$  with an inlet nitroarene flow ( $F$ ) in the range 0.06–0.38  $\text{mmol h}^{-1}$ ; the molar Au ( $n_{\text{Au}}$ ) to  $F$  spanned the range  $2 \times 10^{-3} - 6 \times 10^{-2} \text{ h}$ . In a series of blank tests, passage of each reactant in a stream of  $\text{H}_2$  through the empty reactor did not result in any detectable conversion. The reactor effluent was frozen in a liquid nitrogen trap for subsequent analysis, which was made using a Perkin-Elmer Auto System XL gas chromatograph equipped with a programmed split/splitless injector and flame ionisation detector, employing a DB-1 50 m  $\times$  0.20 mm i.d. 0.33  $\mu\text{m}$  film thickness capillary column (J&W Scientific). Repeated reactions with different samples from the same batch of catalyst delivered raw data that were reproducible to within  $\pm 6\%$  with a carbon balance  $\geq 95\%$ . Taking *p*-nitrobenzonitrile as an example, fractional hydrogenation ( $x_i$ ) was obtained from

$$x_i = \frac{[p\text{-nitrobenzonitrile}]_{\text{in}} - [p\text{-nitrobenzonitrile}]_{\text{out}}}{[p\text{-nitrobenzonitrile}]_{\text{in}}} \quad (2)$$

where selectivity ( $S_i$ ) to *p*-aminobenzonitrile (*p*-ABN) is given by

$$S_i(\%) = \frac{[p\text{-aminobenzonitrile}]_{\text{out}}}{[p\text{-nitrobenzonitrile}]_{\text{in}} - [p\text{-nitrobenzonitrile}]_{\text{out}}} \times 100 \quad (3)$$

### 3. Results and Discussion

#### 3.1 Catalyst Characterisation

It has been shown that calcination in air (at 773 K) is effective in removing residual PVA following the synthesis of bimetallics on alumina.<sup>18</sup> Oxidative treatment is not applicable in the case of Au-Pd/Mo<sub>2</sub>C as the support can undergo deep oxidation with irreversible structural modification at high temperatures. We examined the feasibility of thermal treatment in N<sub>2</sub>, taking Au-Pd/Al<sub>2</sub>O<sub>3</sub>-10 and Au-Pd/Mo<sub>2</sub>C-10 as representative samples. TGA-DSC analysis of Au-Pd/Al<sub>2</sub>O<sub>3</sub>-10 for treatment in air (A) and N<sub>2</sub> (B) resulted in equivalent profiles (Fig. 1). The endothermic response at 328 K (from DSC) is due to the loss of physisorbed water while the exothermic mass loss at higher temperature ( $T > 400$  K) can be attributed to the removal of PVA. The overall change in mass converged (at *ca.* 6 % w/w) in both cases, suggesting equivalence for treatment in air and N<sub>2</sub>. Thermal treatment of Au-Pd/Mo<sub>2</sub>C-10 in N<sub>2</sub> showed comparable behaviour (Fig. 1(C)) with a low and high temperature endothermic and exothermic mass loss. We accordingly applied the same thermal treatment (in N<sub>2</sub> to 773 K) for both alumina and carbide samples. Gold loadings were close to the nominal (1 % w/w) value with Au/Pd atomic ratios approaching the target 30 and 10 in the bimetallic systems (Table 1). Moreover, the Mo/C ratios were close to 2, confirming the synthesis of a Mo<sub>2</sub>C phase with no significant contamination by surface free carbon, which can occlude Mo<sub>2</sub>C active sites and lower activity.<sup>46</sup>

The temperature programmed reduction (TPR) profiles for Au-Pd/Al<sub>2</sub>O<sub>3</sub>-10 and Au-Pd/Mo<sub>2</sub>C-10 are presented in Fig. 2. As the metal component was reduced by NaBH<sub>4</sub> during preparation there was no detectable TPR response for Au-Pd/Al<sub>2</sub>O<sub>3</sub>-10 (Fig. 2(I)). The TPR signal recorded at 437 K for Au-Pd/Mo<sub>2</sub>C-10 (II) can be ascribed to the removal of the passivation layer from the carbide support. This is facilitated by the Pd component with a lower

$T_{max}$  at lower Au/Pd (Table 1). The BET surface area of the carbide systems showed a decrease from 57 to 34 m<sup>2</sup> g<sup>-1</sup> with increasing metal loading that was not evident for the Al<sub>2</sub>O<sub>3</sub> samples. The XRD profile of the latter (taking Au-Pd/Al<sub>2</sub>O<sub>3</sub>-10 as representative (Fig. 3(I)) presented peaks characteristic of  $\delta$ -Al<sub>2</sub>O<sub>3</sub>.<sup>47</sup> The signal at  $2\theta = 77.5^\circ$  can be assigned to Au (311) but the intensity is too weak to allow any meaningful determination of Au particle size from standard line broadening. The XRD pattern for Au-Pd/Mo<sub>2</sub>C-10 (Fig. 3(II)) is consistent with hexagonal  $\beta$ -Mo<sub>2</sub>C, showing characteristic peaks due to (010), (002), (011), (012), (110), (013) and (112) planes. There was no detectable signal for bulk oxide (MoO<sub>3</sub> or MoO<sub>2</sub>), indicating that the precursor had been fully converted to carbide and that passivation resulted in superficial (rather than bulk) oxidation. Gold detection is hampered by overlap with XRD peaks due to the carbide support but the absence of an Au (200) peak at  $44.5^\circ$  suggests a well dispersed Au phase. There was no detectable diffraction peaks due to Pd (notably at  $40.1^\circ$  (111)) in the Au-Pd samples but the Pd loading was too low for detection. The formation of bimetallic nanoparticles has been established in an earlier study using IR spectroscopy coupled with CO adsorption for Au-Pd/Al<sub>2</sub>O<sub>3</sub> prepared by the same method.<sup>18</sup> Villa *et al.* have proposed the generation of bimetallic Au-Pd particles on activated carbon when using PVA as a protecting agent.<sup>48</sup> The presence of isolated Pd atoms surrounded by Au atoms in bimetallic Au-Pd particles is a critical feature of various catalytic reactions using gold-palladium catalysts (*e.g.* hydrogenation<sup>18</sup> and oxidation<sup>44</sup>). The IR spectra (not shown) obtained for the Au-Pd/Al<sub>2</sub>O<sub>3</sub> samples are identical to the ones reported in a previous study<sup>18</sup>. However it was not possible to characterise the Au-Pd/Mo<sub>2</sub>C systems using the same technique because of strong absorption by the dark Mo<sub>2</sub>C material. At this juncture, we assume that the results obtained for the alumina supported catalysts are applicable to the Mo<sub>2</sub>C systems.

Gold particle size is important in hydrogenation application<sup>49</sup> where particles < 5 nm are intrinsically more active in the gas phase hydrogenation of *p*-chloronitrobenzene and *m*-dinitrobenzene<sup>32</sup> and butadiene<sup>50</sup>. Representative TEM images (of Au-Pd/Al<sub>2</sub>O<sub>3</sub>-10 (A) and Au-Pd/Mo<sub>2</sub>C-10 (B)) are presented in Fig. 4(I), where well dispersed pseudo-spherical particles in the 1–8 nm size range (Fig. 4(II)) can be observed. An essentially equivalent mean metal size (4–5 nm) was obtained for all the Al<sub>2</sub>O<sub>3</sub>- and Mo<sub>2</sub>C-supported systems. Previous Au/Mo<sub>2</sub>C synthesis by deposition-precipitation (with urea) generated an appreciably wider size range (4–20 nm) and larger mean (13.4 nm).<sup>34</sup> Application of PVA as stabilising agent was effective in generating homogeneously dispersed nano-particles. Hydrogen dissociation on supported Au has a higher activation energy barrier than conventional hydrogenation metals (Pd, Pt and Ni)<sup>49</sup> and is dependent on Au coordination where dissociation is facilitated at edge and corner sites associated with smaller Au particles (< 10 nm)<sup>33</sup>. Ambient temperature H<sub>2</sub> chemisorption on Au/Al<sub>2</sub>O<sub>3</sub> was low and is in agreement with previous reports.<sup>28,51</sup> Inclusion of Pd resulted in a significant increase in H<sub>2</sub> uptake that was enhanced at lower Au/Pd ratio as observed for catalysts prepared by deposition-precipitation.<sup>34</sup> The higher H<sub>2</sub> chemisorption capacity exhibited by the carbide systems can not be attributed to metal particle size and must be due to additional chemisorption on the Mo<sub>2</sub>C support (Table 1).

The electronic structure of the supported metal can impact on performance in the hydrogenation of nitroarenes<sup>28,52</sup> as –NO<sub>2</sub> adsorption/activation is favoured on electron-deficient sites<sup>28,53</sup>. Electronic character was probed by XPS analysis and the resultant spectra are presented in Fig. 5. The Au 4*f* binding energy (BE) showed a dependence on the support but was unaffected by Pd inclusion (Table 1) where the Au 4*f*<sub>7/2</sub> BE for Al<sub>2</sub>O<sub>3</sub>-supported samples (83.0 eV) was appreciably lower than that (84.2 eV) recorded for the carbide systems (Fig. 5(A)). Previous studies reported that such a shift of the Au 4*f*<sub>7/2</sub> BE to lower energy can be related to a reduced

screening of core holes in an assembly of low-coordinated surface Au atoms<sup>54</sup> or to a reduced coordination number of Au atoms associated with the degree of rounding of Au nanoparticles, which is dependent on metal–support interaction.<sup>55</sup> The equivalent particle size obtained for Au/Al<sub>2</sub>O<sub>3</sub> and Au/Mo<sub>2</sub>C suggests that such effects alone can not account for the variation of Au 4f<sub>7/2</sub> BE. Taking the reference BE for metallic Au as 84.0 eV,<sup>56</sup> the XPS results could also suggest electron transfer from support surface defects to nano-scale Au particles.<sup>57</sup> Previous XPS studies of TiO<sub>2</sub>- and Al<sub>2</sub>O<sub>3</sub>-supported catalysts have indicated metal-support interactions that result in electron transfer from the oxide to supported Au particles.<sup>58</sup> In contrast, the Au 4f<sub>7/2</sub> BE recorded for the carbide systems coincides with the metallic reference, suggesting negligible electron transfer. Care must be taken regarding such interpretation as charging effects in XPS measurements can differ significantly between insulating (Al<sub>2</sub>O<sub>3</sub>) and highly conductive (Mo<sub>2</sub>C) supports. We have observed a Pd 3d<sub>3/2</sub> signal at 340.8 eV for Au-Pd/Mo<sub>2</sub>C-10 (Table 1 and Fig. 5(B)), which is close to the BE reported for metallic Pd 3d<sub>3/2</sub> (at 340.5±0.1 eV)<sup>28,53</sup>. A similar response (Pd 3d<sub>3/2</sub> at 340.9 eV) has been recorded for Pd-Mo<sub>2</sub>C/graphitic carbon.<sup>59</sup> The second signal at 335.7 eV (Fig. 5(B)) can be attributed to Au 4d<sub>5/2</sub> but it should be noted that Au 4d<sub>5/2</sub> and Pd 3d<sub>5/2</sub> XPS signals can overlap, as reported elsewhere<sup>60</sup>. The very low intensity of the XPS signal in the Pd 3d region in the case of Au-Pd/Al<sub>2</sub>O<sub>3</sub>-10 (not shown) precluded detection of a Pd 3d<sub>3/2</sub> contribution. The XPS spectrum over the Mo 3d region (Fig. 5(C)) shows Mo 3d<sub>5/2</sub> peaks at 228.4 and 231.6 eV consistent with a Mo<sub>2</sub>C phase<sup>59,61</sup>. In addition to the carbidic Mo contribution, Mo 3d<sub>5/2</sub> signals at higher BE can be attributed to oxidised states of Mo arising from passivation, *i.e.* Mo(IV) (229.0 eV),<sup>62</sup> Mo(V) (231.2 eV)<sup>63</sup> and Mo(VI) (232.4 eV)<sup>64</sup>. Deconvolution of the C 1s profile (Fig. 5(D)) provides evidence of carbidic (283.4 eV)<sup>65</sup> and graphitic (284.6 eV) carbon<sup>59</sup> with contributions (at 286.3 and 288.6 eV) due to C-O<sup>62</sup> and C=O<sup>66</sup>.

### 3.2 Catalytic Response

This is the first reported application of a Mo<sub>2</sub>C-supported bimetallic (Au-Pd) catalyst in (gas phase) hydrogenation where we examine nitroarene (nitrobenzene, *p*-chloronitrobenzene and *p*-nitrobenzonitrile) conversion, carrying Au/Al<sub>2</sub>O<sub>3</sub> and Au-Pd/Al<sub>2</sub>O<sub>3</sub> through as benchmarks. The target amine products are commercially important in the production of a diversity of agrochemicals, pharmaceuticals and fine chemicals.<sup>67,68</sup> Initial conversion (representative time-on-stream plots shown in Fig. 6(A)) was used to obtain reaction rate (normalised with respect to molar Au loading) using the approach described previously.<sup>69</sup> Reduction of nitrobenzene generated aniline where Au/Mo<sub>2</sub>C outperformed Au/Al<sub>2</sub>O<sub>3</sub> and delivered a greater than three-fold higher rate (Fig. 6(B)). This can be ascribed, at least in part, to the greater available surface hydrogen determined in pulse chemisorption measurements (Table 1) as H<sub>2</sub> activation is rate limiting in hydrogenation over Au. In previous work<sup>32</sup> we established Au particle size effects in –NO<sub>2</sub> hydrogenation with an increase in intrinsic activity with decreasing particle size (from 10 to 3 nm). This should not be a contributory effect here given the equivalency of size distribution and mean. Alumina (without a metal additive) is inactive in hydrogenation whereas Mo<sub>2</sub>C alone can promote H<sub>2</sub> activation with –NO<sub>2</sub> reduction<sup>34</sup> and contribute directly to the higher reaction rate. Incorporation of Pd with Au resulted in increased H<sub>2</sub> chemisorption capacity and a consequent enhanced activity with the highest values recorded for Au/Pd = 10.

Chemoselectivity in amine production is particularly relevant in the hydrogenation of *p*-chloronitrobenzene<sup>70</sup> where a range of intermediates and by-products notably nitrobenzene and aniline have been reported for reaction over Pd and Ni catalysts in both liquid and gas phases<sup>28,53,71,72</sup>. A simplified reaction pathway is presented in Fig. 7(A), where the target *p*-chloroaniline formed *via* –NO<sub>2</sub> reduction (step I) can undergo hydrodechlorination to aniline (step II) or alternatively nitrobenzene is first generated by hydrodechlorination (step III) with

subsequent hydrogenation to aniline (step IV). In previous studies, reaction over Pd/Al<sub>2</sub>O<sub>3</sub> generated nitrobenzene and aniline<sup>28</sup> whereas supported Au was fully selective to chloroaniline<sup>25,27,28,34</sup>. The chemoselectivity achieved with Au catalysts can be attributed to the preferential adsorption of the reactants through the nitro group at the support (notable TiO<sub>2</sub>) and metal/support interface, where the Au (metal) sites provide reactive dissociated H<sub>2</sub>.<sup>73,74</sup> In this study, hydrogenation of *p*-chloronitrobenzene resulted in exclusive *p*-chloroaniline formation with 100% yield over Au-Pd/Mo<sub>2</sub>C-10 and Au-Pd/Mo<sub>2</sub>C-30, *i.e.* full selectivity to *p*-chloroaniline at 100% conversion of the inlet *p*-chloronitrobenzene feed. This result is of importance as we previously observed that the incorporation of Pd on Au/Al<sub>2</sub>O<sub>3</sub> (Au/Pd = 8) favoured hydrodechlorination with formation of nitrobenzene.<sup>3</sup> Performance must be influenced by catalyst synthesis where the colloidal method with PVA used here has been shown to generate surface isolated Pd atoms (Pd monomers) surrounded by Au atoms in bimetallic particles.<sup>18</sup> This effect appears to extend to the carbide system. In contrast, preparation by deposition-precipitation results in segregated Pd sites that promote hydrodechlorination at low Au/Pd ratio.<sup>3</sup> This is consistent with the observation of Gao *et al.*<sup>7</sup> that enhanced selectivity/activity (in H<sub>2</sub>O<sub>2</sub>/vinyl acetate synthesis) was attributed to an “ensemble effect” resulting from dilution of surface Pd by Au which was dependent on Au content. The Mo<sub>2</sub>C-supported catalysts again generated appreciably higher rates than the equivalent alumina-supported samples (Fig. 6(C)) with increased activity resulting from the inclusion of Pd.

Catalytic performance was further assessed in the gas phase hydrogenation of *p*-nitrobenzonitrile. The limited available literature<sup>67,75-77</sup> refers to batch liquid phase reactions at elevated pressures (up to 6 MPa) where high selectivity to *p*-aminobenzonitrile has proved challenging. Koprivova and Cervený<sup>76</sup> identified 15 possible intermediates and products that involve disproportionation, reduction, condensation, hydrodenitrogenation and

hydrodecarbonation reactions. A reaction pathway that includes the major reported products<sup>76,77</sup> is presented in Fig. 7(B). Conversion of *p*-nitrobenzonitrile to the target *p*-aminobenzonitrile (step I) can be accompanied by further hydrogenation/hydration to *p*-aminobenzamide (step II) or hydrogenation to *p*-aminobenzylamine (step II)<sup>76</sup> with subsequent hydrogenolysis to *p*-aminotoluene (step IV)<sup>76,77</sup>. In recent work we have established that oxide supported Pd and Ni are nonselective, generating *p*-aminotoluene as by-product.<sup>78</sup> Each catalyst in this study was fully selective to *p*-aminobenzonitrile with 100% yield over Au-Pd/Mo<sub>2</sub>C-10 and Au-Pd/Mo<sub>2</sub>C-30, exceeding the highest reported values for supported Au (96-97% over Au/TiO<sub>2</sub><sup>67</sup> and Au/Fe<sub>2</sub>O<sub>3</sub><sup>75</sup>) operated in batch liquid phase at elevated pressure (25 bar H<sub>2</sub>). Economies of scale favour continuous processes for high throughput.<sup>25</sup> Palladium again served as promoter with higher rates recorded for the carbide catalysts (Fig. 6(D)). The only reported gas phase catalysis study dates from the 1950s where Hata and Watanabe<sup>77</sup> investigated the hydrogenation of various aromatic nitriles (including the three nitrobenzonitrile isomers) over a Ni–Cu catalyst at 523-573 K and reported, as principal products, aniline, toluidine and aminobenzonitrile (< 32% yield). Our results represent a significant advance in the sustainable production of a target amine where reaction exclusivity at full reactant conversion removes the requirement for energy intensive down-stream separation/purification unit operations.

#### 4. Conclusions

We provide the first reported synthesis of Mo<sub>2</sub>C-supported (Au-Pd) bimetallic catalysts used to promote the gas phase hydrogenation of nitroarenes (nitrobenzene, *p*-chloronitrobenzene and *p*-nitrobenzonitrile). The Mo<sub>2</sub>C support was synthesised by temperature programmed carburisation (of H<sub>2</sub>MoO<sub>4</sub> in CH<sub>4</sub>/H<sub>2</sub>) and confirmed by XRD analysis. Bimetallic catalyst synthesis with Au and Pd colloids employed polyvinyl alcohol (PVA) as stabiliser to avoid



agglomeration and resulted in nano-scale (1-8 nm size range) supported metal particles with mean size of 4-5 nm. The bimetallic catalysts exhibited increased H<sub>2</sub> chemisorption capacity with higher uptake on Au-Pd/Mo<sub>2</sub>C relative to Au-Pd/Al<sub>2</sub>O<sub>3</sub>. XPS analysis suggests electron donation from Al<sub>2</sub>O<sub>3</sub> to Au whereas the BE recorded for Au on Mo<sub>2</sub>C (for both monometallic and Au-Pd bimetallic systems) was close to the metallic Au reference. All the catalysts were 100% selective in –NO<sub>2</sub> hydrogenation to the target amine. The Mo<sub>2</sub>C-supported Au system exhibited a higher (greater than 3-fold) hydrogenation rate that was further enhanced by addition of Pd (Au/Pd from 30 to 10), which can be attributed to an increase in available surface reactive hydrogen. We achieved 100% amine yield over Au-Pd/Mo<sub>2</sub>C-10 and Au-Pd/Mo<sub>2</sub>C-30 in continuous operation. The results have established controlled preparation of well dispersed Au-Pd on Mo<sub>2</sub>C and application in the clean continuous production of high value amines.

### Acknowledgements

Financial support to Dr. X. Wang through the Overseas Research Students Award Scheme (ORSAS) is acknowledged. Dr. N. Perret also acknowledges financial support from COST Action MP0903 Nanoalloys.

### References

1. F. Tao, *Chem. Soc. Rev.*, 2012, **41**, 7977-7979.
2. R. W. J. Scott, O. M. Wilson, S.-K. Oh, E. A. Kenik and R. M. Crooks, *J. Am. Chem. Soc.*, 2004, **126**, 15583-15591.
3. F. Cárdenas-Lizana, S. Gómez-Quero, A. Hugon, L. Delannoy, C. Louis and M. A. Keane, *J. Catal.*, 2009, **262**, 235-243.
4. S. Chandra Shekar, J. Krishna Murthy, P. Kanta Rao, K. S. Rama Rao and E. Kemnitz, *Appl. Catal. A: Gen.*, 2003, **244**, 39-48.
5. F. Menegazzo, P. Canton, F. Pinna and N. Pernicone, *Catal. Commun.*, 2008, **9**, 2353-2356.
6. V. Dal Santo, A. Gallo, A. Naldoni, M. Guidotti and R. Psaro, *Catal. Today*, 2012, **197**, 190-205.
7. F. Gao and D. W. Goodman, *Chem. Soc. Rev.*, 2012, **41**, 8009-8020.
8. P. Gao, F. Li, F. Xiao, N. Zhao, N. Sun, W. Wei, L. Zhong and Y. Sun, *Catal. Sci. Technol.*, 2012, **2**, 1447-1454.

9. D.-W. Lee, M. S. Lee, J. Y. Lee, S. Kim, H.-J. Eom, D. J. Moon and K.-Y. Lee, *Catal. Today*, 2013, **210**, 2-9.
10. F. Menegazzo, M. Signoretto, M. Manzoli, F. Boccuzzi, G. Cruciani, F. Pinna and G. Strukul, *J. Catal.*, 2009, **268**, 122-130.
11. X. Wei, X.-F. Yang, A.-Q. Wang, L. Li, X.-Y. Liu, T. Zhang, C.-Y. Mou and J. Li, *J. Phys. Chem. C*, 2010, **116**, 6222-6232.
12. M. L. Guzmán-Castillo, E. López-Salinas, J. J. Fripiat, J. Sánchez-Valente, F. Hernández-Beltrán, A. Rodríguez-Hernández and J. Navarrete-Bolaños, *J. Catal.*, 2003, **220**, 317-325.
13. M. O. Nutt, K. N. Heck, P. Alvarez and M. S. Wong, *Appl. Catal. B: Environ.*, 2006, **69**, 115-125.
14. C. L. Bianchi, P. Canton, N. Dimitratos, F. Porta and L. Prati, *Catal. Today*, 2005, **102-103**, 203-212.
15. F. Gao, Y. Wang and D. W. Goodman, *J. Am. Chem. Soc.*, 2009, **131**, 5734-5735.
16. A. Villa, N. Janjic, P. Spontoni, D. Wang, D. S. Su and L. Prati, *Appl. Catal. A: Gen.*, 2009, **364**, 221-228.
17. A. Hugon, L. Delannoy, J.-M. Krafft and C. Louis, *J. Phys. Chem. C*, 2010, **114**, 10823-10835.
18. N. E. Kolli, L. Delannoy and C. Louis, *J. Catal.*, 2013, **297**, 79-92.
19. B. Pawelec, A. M. Venezia, V. La Parola, E. Cano-Serrano, J. M. Campos-Martin and J. L. G. Fierro, *Appl. Surf. Sci.*, 2005, **242**, 380-391.
20. A. M. Venezia, V. L. Parola, B. Pawelec and J. L. G. Fierro, *Appl. Catal. A: Gen.*, 2004, **264**, 43-51.
21. A. Sárkány, O. Geszti and G. Sáfrán, *Appl. Catal. A: Gen.*, 2008, **350**, 157-163.
22. X. Yang, D. Chen, S. Liao, H. Song, Y. Li, Z. Fu and Y. Su, *J. Catal.*, 2012, **291**, 36-43.
23. P. Weinberger, L. Szunyogh and B. I. Bennett, *Phys. Rev. B*, 1993, **47**, 10154-10157.
24. A. Groß, *Top. Catal.*, 2006, **37**, 29-39.
25. X. Wang, F. Cárdenas-Lizana and M. A. Keane, *ACS Sustainable Chem. Eng.*, 2014, **2**, 2781-2789.
26. X. Wang, N. Perret and M. A. Keane, *Appl. Catal. A: Gen.*, 2013, **467**, 575-584.
27. X. Wang, N. Perret, J. J. Delgado, G. Blanco, X. Chen, C. M. Olmos, S. Bernal and M. A. Keane, *J. Phys. Chem. C*, 2013, **117**, 994-1005.
28. X. Wang, N. Perret and M. A. Keane, *Chem. Eng. J.*, 2012, **210**, 103-113.
29. H. Liu, K. Tao, C. Xiong and S. Zhou, *Catal. Sci. Technol.*, 2015, **5**, 405-414.
30. M. Pietrowski and M. Wojciechowska, *Catal. Today*, 2009, **142**, 211-214.
31. N. Perret, F. Cárdenas-Lizana and M. A. Keane, *Catal. Commun.*, 2011, **16**, 159-164.
32. X. Wang, M. Li and M. A. Keane, in *Heterogeneous Gold Catalysts and Catalysis*, eds. Z. Ma and S. Dai, The Royal Society of Chemistry, Cambridge, 2014, pp. 424-461.
33. E. Bus, J. T. Miller and J. A. van Bokhoven, *J. Phys. Chem. B*, 2005, **109**, 14581-14587.
34. N. Perret, X. Wang, L. Delannoy, C. Potvin, C. Louis and M. A. Keane, *J. Catal.*, 2012, **286**, 172-183.
35. D. Wang and Y. Li, *Adv. Mater.*, 2011, **23**, 1044-1060.
36. J. K. Edwards, A. Thomas, A. F. Carley, A. A. Herzing, C. J. Kiely and G. J. Hutchings, *Green Chem.*, 2008, **10**, 388-394.
37. J. K. Edwards, B. Solsona, P. Landon, A. F. Carley, A. Herzing, M. Watanabe, C. J. Kiely and G. J. Hutchings, *J. Mater. Chem.*, 2005, **15**, 4595-4600.
38. J. K. Edwards, B. E. Solsona, P. Landon, A. F. Carley, A. Herzing, C. J. Kiely and G. J. Hutchings, *J. Catal.*, 2005, **236**, 69-79.

39. J. Xu, T. White, P. Li, C. He, J. Yu, W. Yuan and Y.-F. Han, *J. Am. Chem. Soc.*, 2010, **132**, 10398-10406.
40. P. Zhao, N. Li and D. Astruc, *Coordin. Chem. Rev.*, 2013, **257**, 638-665.
41. S. Yongprapat, A. Therdthianwong and S. Therdthianwong, *J. Appl. Electrochem.*, 2012, **42**, 483-490.
42. J. M. Nadgeri, M. M. Telkar and C. V. Rode, *Catal. Commun.*, 2008, **9**, 441-446.
43. Y. S. Kwon, A. A. Gromov, A. P. Ilyin, A. A. Ditts, J. S. Kim, S. H. Park and M. H. Hong, *Int. J. Refract. Met. Hard Mater.*, 2004, **22**, 235-241.
44. D. Wang, A. Villa, F. Porta, L. Prati and D. Su, *J. Phys. Chem. C*, 2008, **112**, 8617-8622.
45. F. Cárdenas-Lizana, X. Wang, D. Lamey, M. Li, M. A. Keane and L. Kiwi-Minsker, *Chem. Eng. J.*, 2014, **255**, 695-704.
46. J.-S. Choi, G. Bugli and G. Djéga-Mariadassou, *J. Catal.*, 2000, **193**, 238-247.
47. I. Pettiti, S. Colonna, S. De Rossi, M. Faticanti, G. Minelli and P. Porta, *Phys. Chem. Chem. Phys.*, 2004, **6**, 1350-1358.
48. A. Villa, D. Wang, D. Su, G. M. Veith and L. Prati, *Phys. Chem. Chem. Phys.*, 2010, **12**, 2183-2189.
49. G. C. Bond, C. Louis and D. T. Thompson, *Catalysis by Gold*, Imperial College Press, London, 2006.
50. A. Hugon, L. Delannoy and C. Louis, *Gold Bull.*, 2008, **41**, 127-138.
51. P. Claus, *Appl. Catal. A: Gen.*, 2005, **291**, 222-229.
52. S. A. Nikolaev and V. Smirnov, *Gold Bull.*, 2009, **42**, 182-189.
53. F. Cardenas-Lizana, Y. Hao, M. Crespo-Quesada, I. Yuranov, X. Wang, M. A. Keane and L. Kiwi-Minsker, *ACS Catal.*, 2013, **3**, 1386-1394.
54. A. Zwiijnenburg, A. Goossens, W.G. Sloof, M.W.J. Craje, A.M. van der Kraan, L.J. de Jongh, M. Makkee and J.A. Moulijn, *J. Phys. Chem. B*, 2002, **106**, 9853-9862.
55. J. Radnik, C. Mohr and P. Claus, *Phys. Chem. Chem. Phys.*, 2003, **5**, 172-177.
56. M. Baron, O. Bondarchuk, D. Stacchiola, S. Shaikhutdinov and H. J. Freund, *J. Phys. Chem. C*, 2009, **113**, 6042-6049.
57. Z. Jiang, W. Zhang, L. Jin, X. Yang, F. Xu, J. Zhu and W. Huang, *J. Phys. Chem. C* 2007, **111**, 12434-12439.
58. S. Arrii, F. Morfin, A. J. Renouprez and J. L. Rousset, *J. Am. Chem. Soc.*, 2004, **126**, 1199-1205.
59. R. Wang, J. Yang, K. Shi, B. Wang, L. Wang, G. Tian, B. Bateer, C. Tian, P. Shen and H. Fu, *RSC Adv.*, 2013, **3**, 4771-4777.
60. C. Yang, A. K. Manocchi, B. Lee and H. Yi, *J. Mater. Chem.*, 2011, **21**, 187-194.
61. R. Barthos, A. Szechenyi and F. Solymosi, *Catal. Lett.*, 2008, **120**, 161-165.
62. A. C. Lausche, J. A. Schaidle and L. T. Thompson, *Appl. Catal. A: Gen.*, 2011, **401**, 29-36.
63. M. Shimoda, T. Hirata, K. Yagisawa, M. Okochi and A. Yoshikawa, *J. Mater. Sci. Lett.*, 1989, **8**, 1089-1091.
64. Z. B. Z. Wei, P. Grange and B. Delmon, *Appl. Surf. Sci.*, 1998, **135**, 107-114.
65. T. P. St. Clair, S. T. Oyama, D. F. Cox, S. Otani, Y. Ishizawa, R.-L. Lo, K.-i. Fukui and Y. Iwasawa, *Surf. Sci.*, 1999, **426**, 187-198.
66. S. J. Ardakani, X. Liu and K. J. Smith, *Appl. Catal. A: Gen.*, 2007, **324**, 9-19.
67. A. Corma, C. González-Arellano, M. Iglesias and F. Sánchez, *Appl. Catal. A: Gen.*, 2009, **356**, 99-102.
68. H.-U. Blaser, H. Steiner and M. Studer, *ChemCatChem*, 2009, **1**, 210-221.

69. N. Perret, X. Wang, T. Onfroy, C. Calers and M. A. Keane, *J. Catal.*, 2014, **309**, 333-342.
70. C. Xiao, X. Wang, C. Lian, H. Liu, M. Liang and Y. Wang, *Curr. Org. Chem.*, 2012, **16**, 280-296.
71. J.-F. Su, B. Zhao and Y.-W. Chen, *Ind. Eng. Chem. Res.*, 2011, **50**, 1580-1587.
72. B. Zhao and Y.-W. Chen, *J. Non-Cryst. Solids*, 2010, **356**, 839-847.
73. M. Boronat, P. Concepción, A. Corma, S. González, F. Illas and P. Serna, *J. Am. Chem. Soc.*, 2007, **129**, 16230-16237.
74. A. Corma, M. Boronat, S. Gonzalez and F. Illas, *Chem. Commun.*, 2007, 3371-3373.
75. A. Corma and P. Serna, *Science*, 2006, **313**, 332-334.
76. K. Koprivova and L. Cervený, *Res. Chem. Intermed.*, 2008, **34**, 93-101.
77. K. Hata and K.-I. Watanabe, *B. Chem. Soc. Jpn.*, 1959, **32**, 861-867.
78. X. Wang, Y. Hao and M. A. Keane, *Appl. Catal. A: Gen.*, 2016, **510**, 171-179.

**Table 1:** Gold content (% w/w), Au/Pd and Mo/C ratios, BET surface area, temperature related H<sub>2</sub> consumption maximum during TPR ( $T_{max}$ ), metal particle size range and surface area weighted mean diameter ( $d$ ), H<sub>2</sub> chemisorption and XPS binding energies (BE) for Au 4f<sub>7/2</sub>, Pd 3d<sub>3/2</sub> and Mo 3d<sub>5/2</sub>.

	Au (% w/w)	Molar ratio		BET area (m <sup>2</sup> g <sup>-1</sup> )	TPR $T_{max}$ (K)	Particle size (nm)		H <sub>2</sub> chemisorption (μmol g <sup>-1</sup> )	BE XPS (eV)	
		Au/Pd	Mo/C			range	mean ( $d$ )		Au 4f <sub>7/2</sub>	Mo 3d <sub>5/2</sub>
Au/Al <sub>2</sub> O <sub>3</sub>	0.94	-	-	104	-	1-8	5.4	0.4	83.0	-
Au-Pd/Al <sub>2</sub> O <sub>3</sub> -30	0.97	27	-	100	-	1-8	4.6	0.7	-	-
Au-Pd/Al <sub>2</sub> O <sub>3</sub> -10	0.95	9	-	101	-	1-7	4.5	1.2	83.0	-
Mo <sub>2</sub> C	-	-	1.95	57	500	1-7	-	0.4	-	228.4
Au/Mo <sub>2</sub> C	0.81	-	1.95	42	493	1-7	4.3	1.0	84.2	228.4
Au-Pd/Mo <sub>2</sub> C-30	0.87	32	2.00	38	476	1-7	4.2	1.5	-	-
Au-Pd/Mo <sub>2</sub> C-10	0.84	14	1.96	34	437	1-7	4.3	2.1	84.2 (340.8 <sup>a</sup> )	228.4

<sup>a</sup>Pd 3d<sub>3/2</sub>

### Figure Captions

**Fig. 1:** TGA (solid line) and DSC (dashed line) profiles generated in the pre-treatment of (A) Au-Pd/Al<sub>2</sub>O<sub>3</sub>-10 in air, (B) Au-Pd/Al<sub>2</sub>O<sub>3</sub>-10 in N<sub>2</sub> and (C) Au-Pd/Mo<sub>2</sub>C-10 in N<sub>2</sub>; 100 cm<sup>3</sup> min<sup>-1</sup> gas flow at 10 K min<sup>-1</sup> to 373 K (held for 1 h) and then to 773 K.

**Fig. 2:** Temperature programmed reduction (TPR) profiles for Au-Pd/Al<sub>2</sub>O<sub>3</sub>-10 (I) and Au-Pd/Mo<sub>2</sub>C-10 (II).

**Fig. 3:** XRD patterns for Au-Pd/Al<sub>2</sub>O<sub>3</sub>-10 (I) and Au-Pd/Mo<sub>2</sub>C-10 (II). Peak assignments are based on JCPDS-ICDD reference standards:  $\delta$ -Al<sub>2</sub>O<sub>3</sub> (●, 16-394);  $\beta$ -Mo<sub>2</sub>C (■, 11-0680); Au (▲, 04-0784).

**Fig. 4:** Representative TEM images (I) with associated particle size distribution (II) for Au-Pd/Al<sub>2</sub>O<sub>3</sub>-10 (A) and Au-Pd/Mo<sub>2</sub>C-10 (B).

**Fig. 5:** XPS spectra: (A) over the Au 4*f* region for Au-Pd/Al<sub>2</sub>O<sub>3</sub>-10 (I) and Au-Pd/Mo<sub>2</sub>C-10 (II); (B) over the Au 4*d* and Pd 3*d* region for Au-Pd/Mo<sub>2</sub>C-10; (C) with peak deconvolution over the Mo 3*d* region for Au-Pd/Mo<sub>2</sub>C-10; (D) with peak deconvolution over the C 1*s* region for Au-Pd/Mo<sub>2</sub>C-10.

**Fig. 6:** (A) Variation of NB fractional conversion ( $x_i$ ) over Au/Mo<sub>2</sub>C (■), *p*-CNB over Au-Pd/Mo<sub>2</sub>C-30 (●) and *p*-NBN over Au-Pd/Mo<sub>2</sub>C-10 (▲) with time on-stream. Reaction rate ( $r$ ) with associated selectivity ( $S_i$ ) to the target amines (aniline, *p*-chloroaniline and *p*-aminobenzonitrile) in the hydrogenation of (B) nitrobenzene, (C) *p*-chloronitrobenzene and (D) *p*-nitrobenzonitrile.

**Fig. 7:** Reaction pathways for (A) *p*-chloronitrobenzene and (B) *p*-nitrobenzonitrile hydrogenation.

Fig. 1

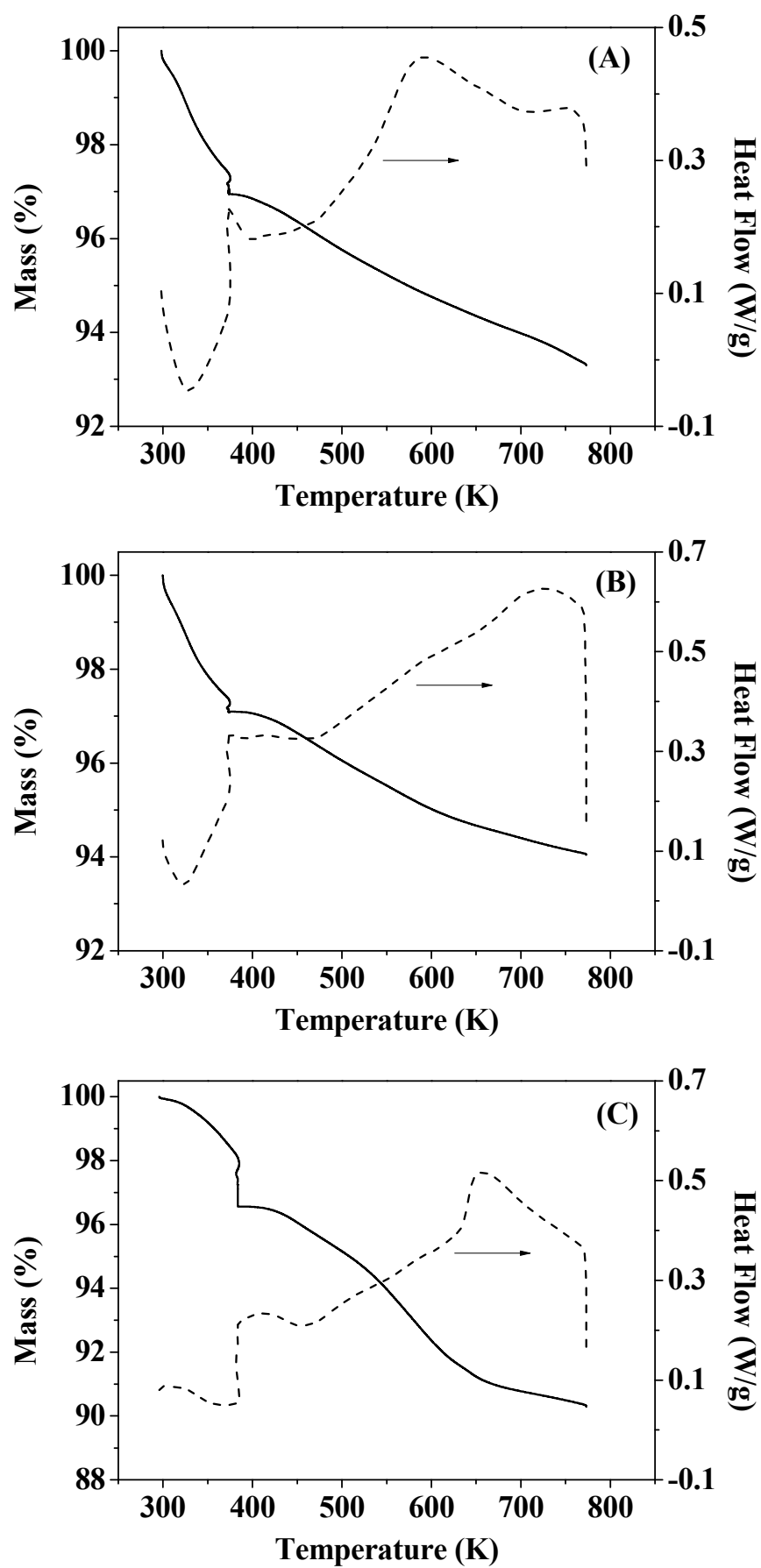


Fig. 2

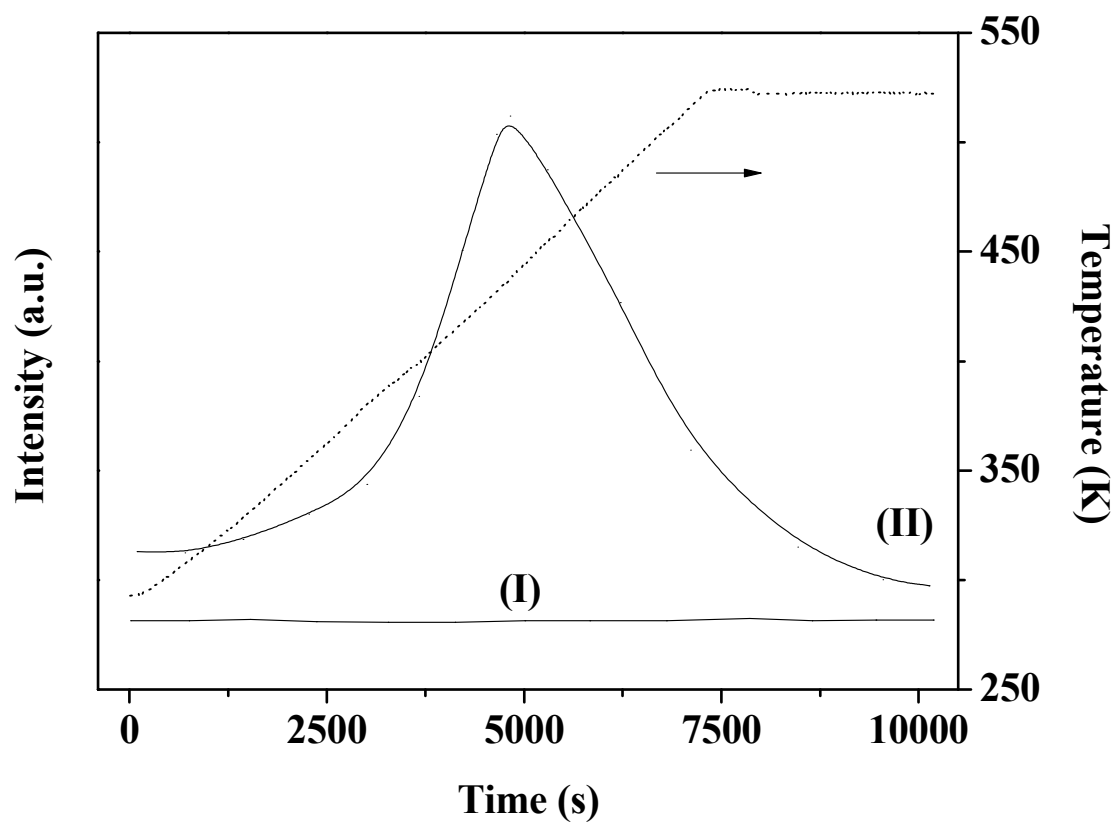




Fig. 3

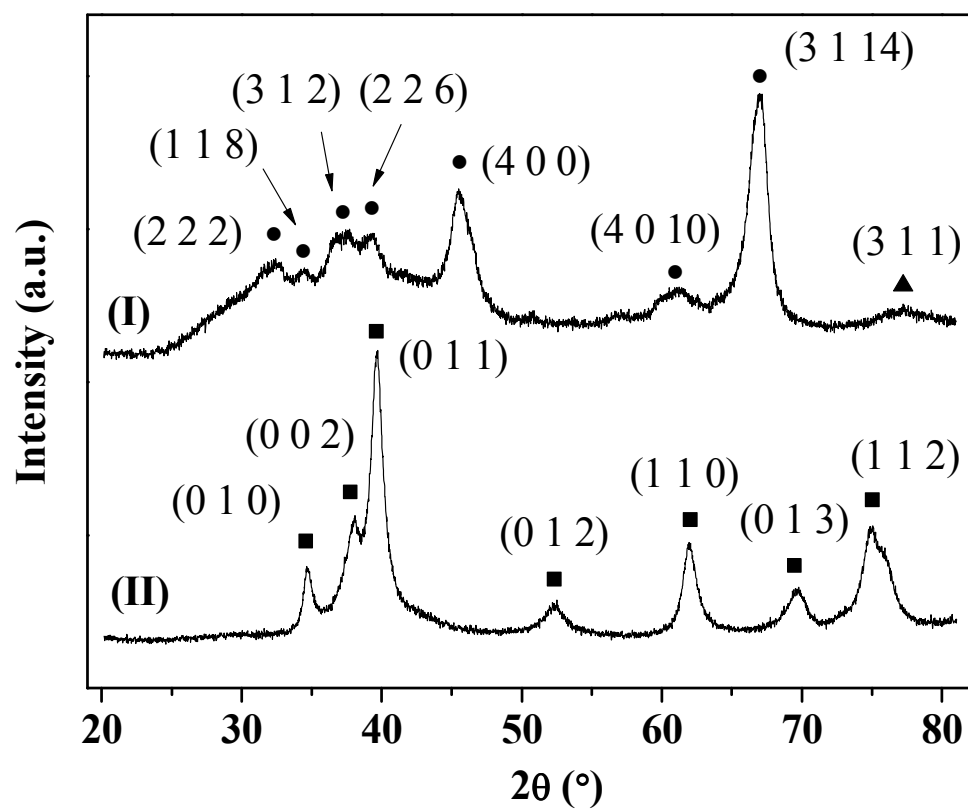


Fig. 4

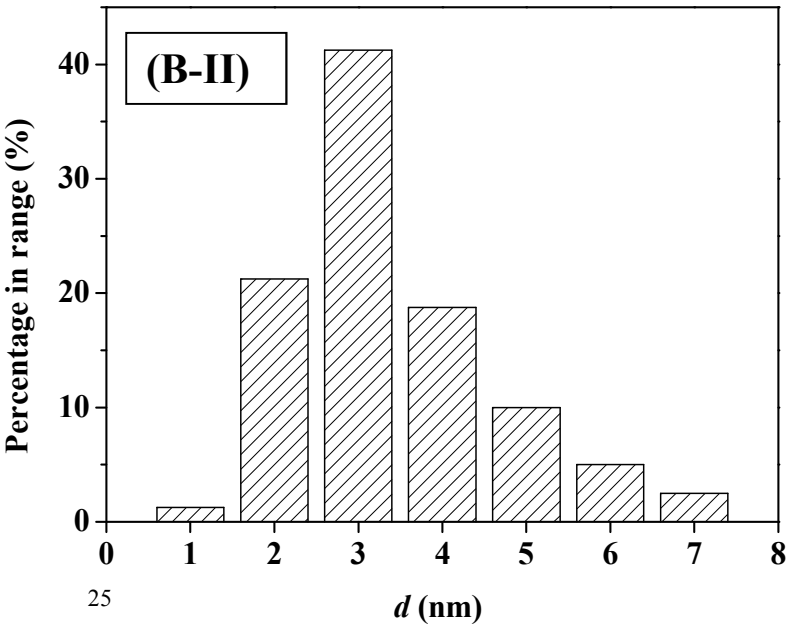
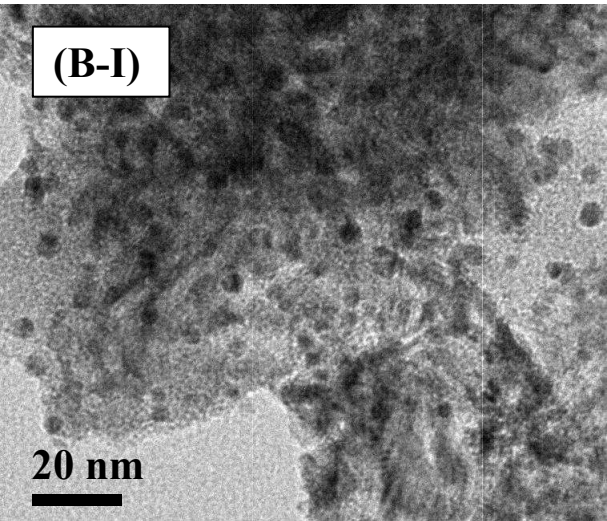
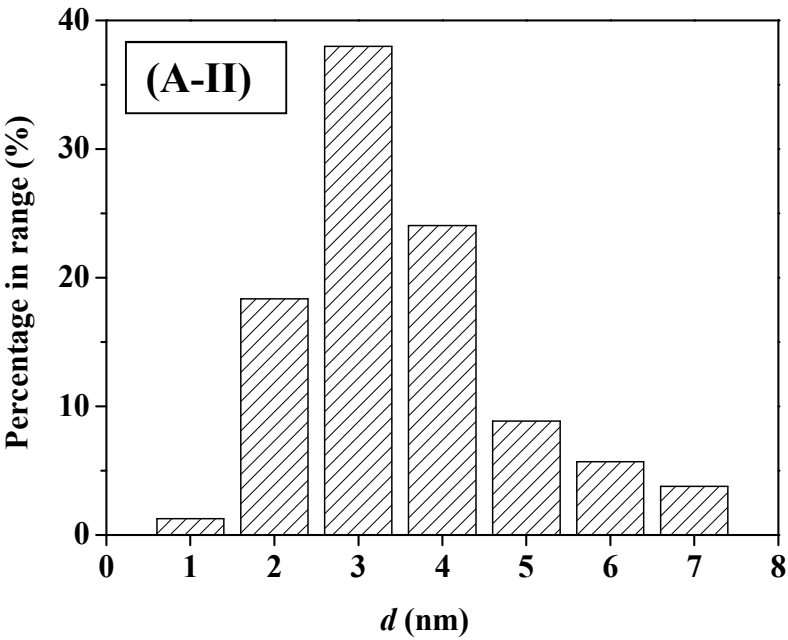
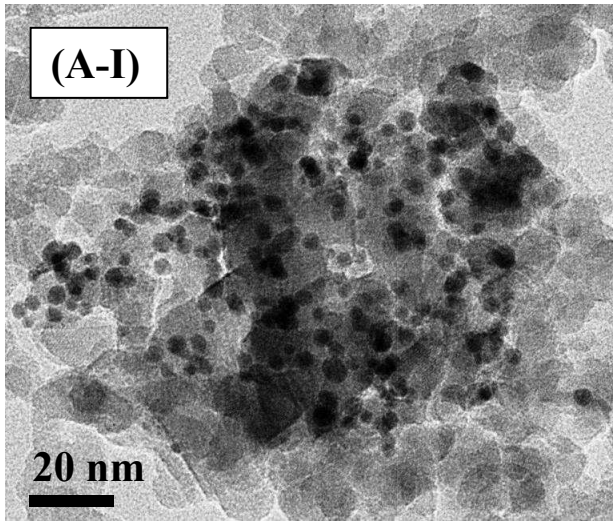


Fig. 5

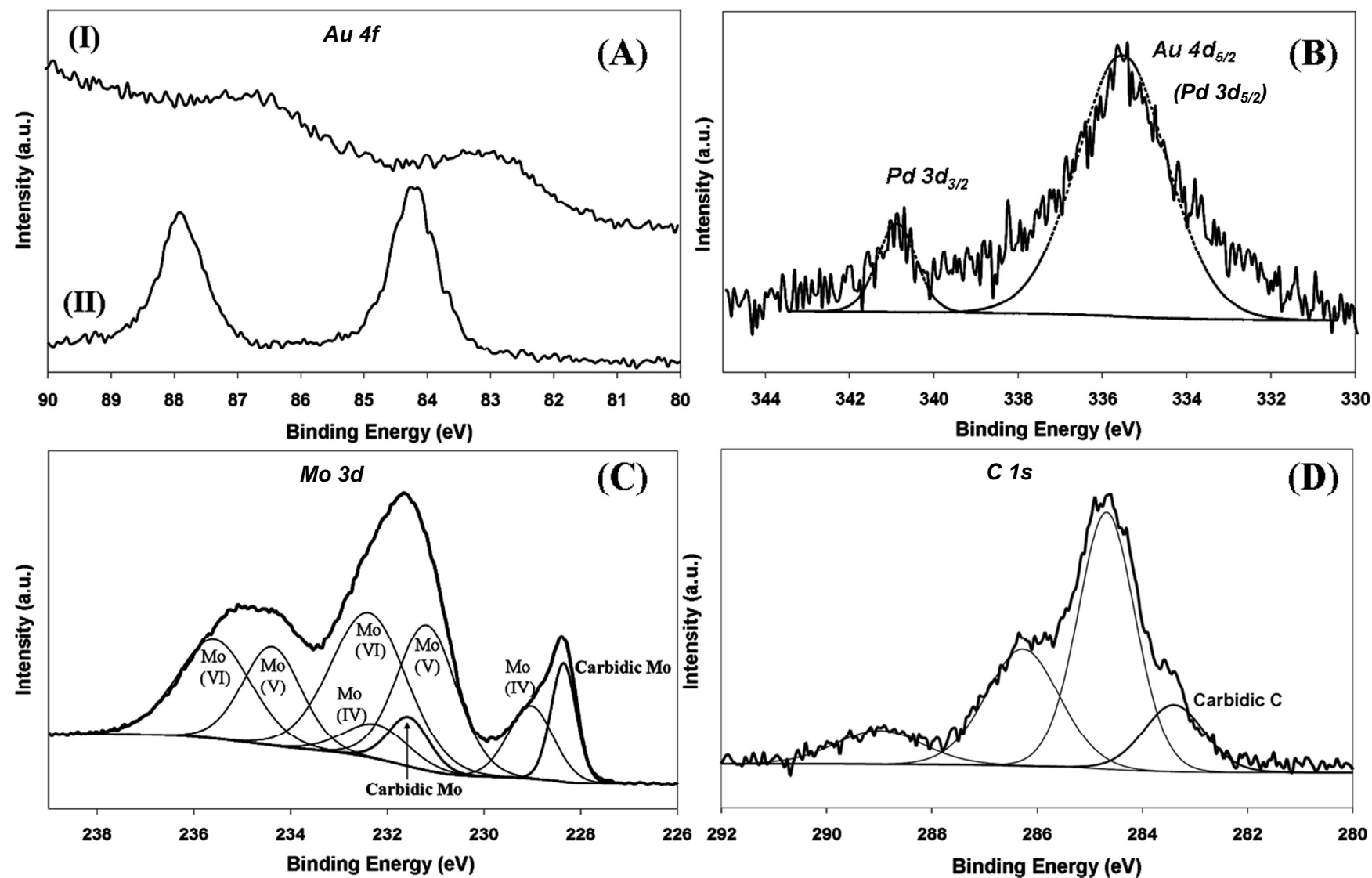


Fig. 6

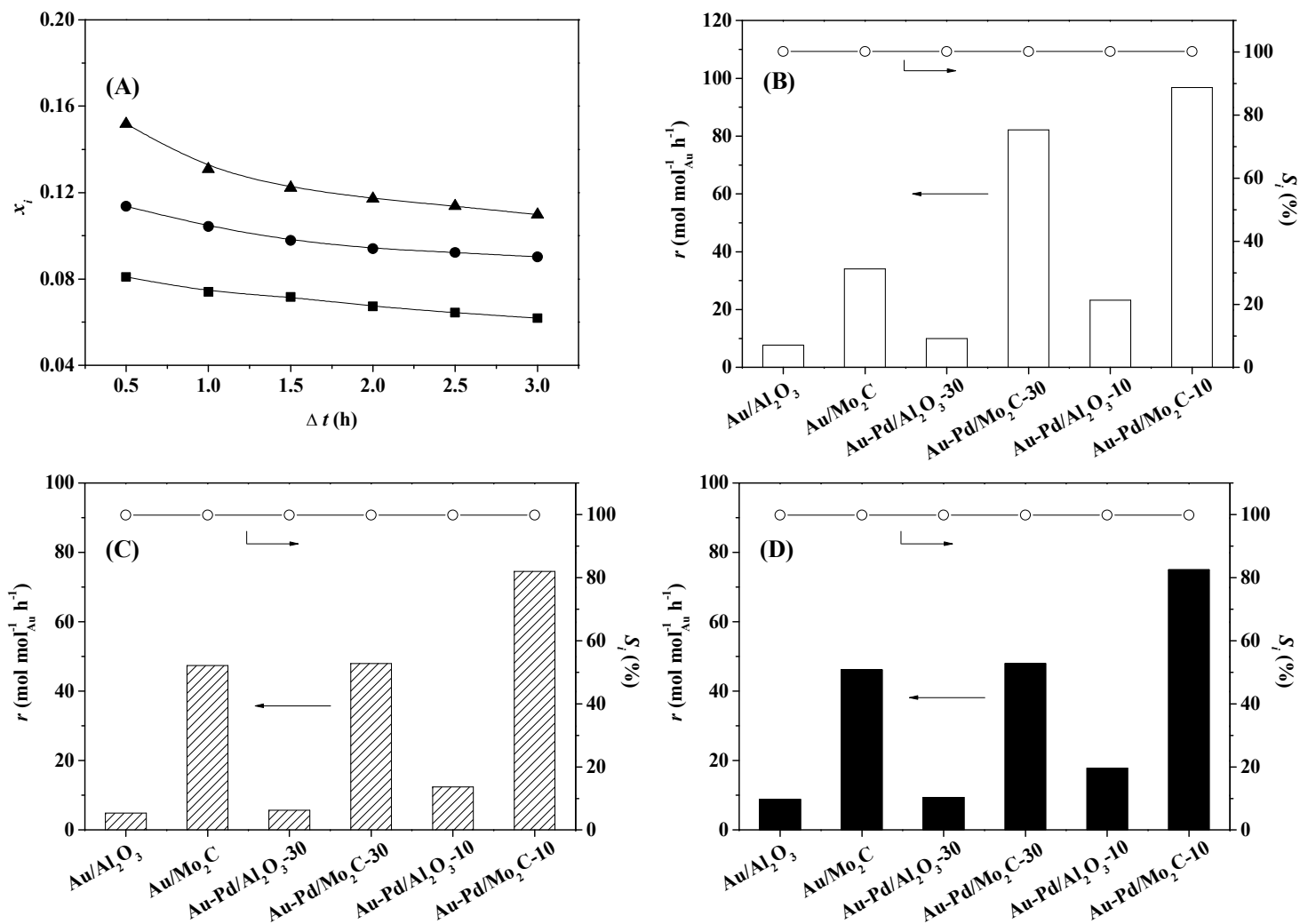
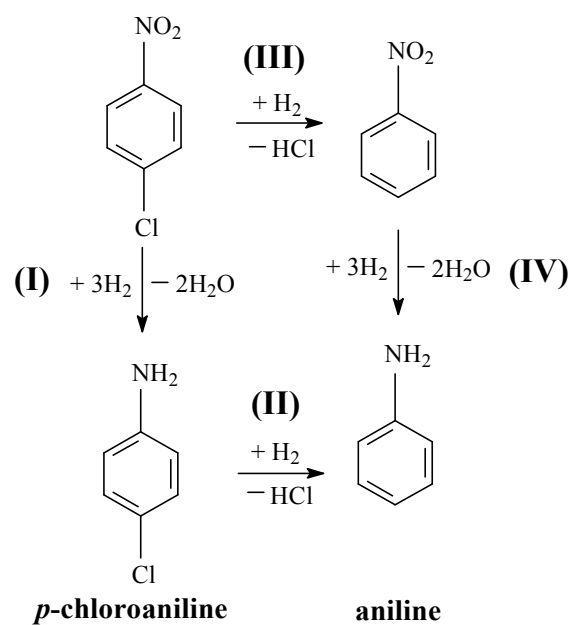
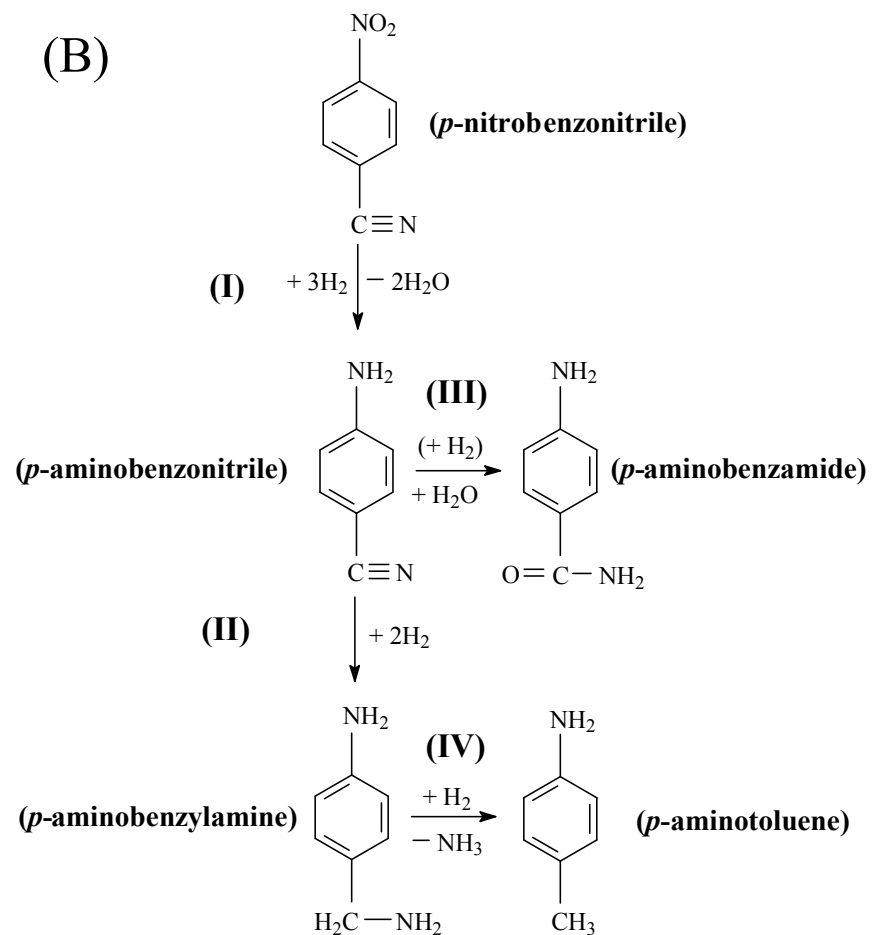


Fig. 7

(A) *p*-chloronitrobenzene      nitrobenzene

(B)



Selective Gas Phase Hydrogenation of Nitroarenes over Mo<sub>2</sub>C Supported Au-Pd

Xiaodong Wang, Noémie Perret, Laurent Delannoy,  
Catherine Louis and Mark A. Keane

First reported synthesis of Au-Pd/Mo<sub>2</sub>C from colloidal nanoparticles with enhanced selective catalytic hydrogenation of functionalised nitroarenes.

